

Article

Estimation of Shallow Sulphur Deposit Resources Based on Reflection Seismic Studies and Well Logging

Kamil Cichostępski *  and Jerzy Dec * 

Department of Geophysics, Faculty of Geology, Geophysics and Environmental Protection,
AGH University of Science and Technology, Mickiewicza 30, 30059 Kraków, Poland

* Correspondence: kcichy@agh.edu.pl (K.C.); geodec@agh.edu.pl (J.D.)

Abstract: In this article we present a novel method for the estimation of sulphur deposit resources based on high-resolution shallow reflection seismic survey and well logging. The study area was sited in the northern part of the Carpathian Foredeep (SE Poland), where sulphur ore occurs in carbonate rocks at a depth of about 120 m, with a thickness of approximately 25 m. The results of many years of seismic monitoring performed in the area of the sulphur deposit allowed us to determine the quantitative relationships between the amplitude of the seismic signal reflected from the top of the deposit and its petrophysical parameters such as porosity and sulphur content. The method of evaluating sulphur deposit is based on extensive statistics concerning the reservoir properties obtained from borehole data. We also discuss a methodology for conducting field acquisition and processing of seismic data in the aspect of mapping the actual amplitudes of the signal reflected from the top of a deposit. The results of estimating the abundance of carbonate sulphur deposits are presented based on the example of a seismic cross-section from the Osiek sulphur mine. Obtained results allow indicating the most prospective zones suitable for exploitation.



Citation: Cichostępski, K.; Dec, J. Estimation of Shallow Sulphur Deposit Resources Based on Reflection Seismic Studies and Well Logging. *Energies* **2021**, *14*, 5323. <https://doi.org/10.3390/en14175323>

Academic Editors: Yangkang Chen and Nikolaos Koukouzas

Received: 4 August 2021

Accepted: 25 August 2021

Published: 27 August 2021

Publisher's Note: MDPI stays neutral with regard to jurisdictional claims in published maps and institutional affiliations.



Copyright: © 2021 by the authors. Licensee MDPI, Basel, Switzerland. This article is an open access article distributed under the terms and conditions of the Creative Commons Attribution (CC BY) license (<https://creativecommons.org/licenses/by/4.0/>).

Keywords: sulphur ore deposit; high-resolution shallow reflection seismic; acquisition design; seismic imaging of carbonate deposit

1. Introduction

Sulphur, as a raw material, has had seen extensive application over the centuries. It is used in the production of pharmaceuticals, medicine, gunpowder and wine, in the rubber industry and in the chemical industry in the broadest sense. The basic product obtained from sulphur is sulphuric acid, which is one of the main components of many further chemical processes, such as the production of artificial fertilisers.

In recent years, the world economy has seen a dramatic decline in the extraction of native sulphur. As extracting fossil native sulphur is expensive, it is being replaced by cheaply obtained sulphur recovered from sulphurised natural gas and oil deposits. However, native sulphur deposits are still a source of sulphur in international trade, especially for local needs.

Polish native sulphur resources are among the largest in the world [1–3]. They occur in the marginal part of the Carpathian Foredeep (south-eastern Poland) at depths of about 100 to 300 m. They are associated with a Tertiary chemical formation that consists of limestone, marly limestone and marl with clay materials. The sulphur occurs in small caverns and fissures and its content is on average 25–30%, but it can reach 70%. It is formed through the reduction of sulphates (mainly gypsum and anhydrite) with the participation of bacteria and hydrocarbons [4–6]. In 2020, Poland's documented sulphur deposits were estimated at 494.08 million tons [7]. Currently, of the 16 known and exploited deposits in the past, the mining of native sulphur in Poland has been carried out for a long time only from the Osiek deposit. However, the year 2019 saw the recommencement of exploitation of the Basznia deposit, abandoned many years previously.

The authors have conducted seismic monitoring of the Osiek deposit for many years [8–12] and carried out reconnaissance of the Basznia deposit [13]. Seismic imaging makes it possible to determine the structure and petrophysical properties of the deposit and help locate suitable exploitation sites. In sulphur mining regions, monitoring of the dynamic processes occurring under the influence of exploiting the deposit and its overburden makes it possible to conduct environmentally safe mining activities. Long-term studies of the Osiek sulphur deposit have made it possible to determine quantitative relationships between the amplitude of the seismic signal recorded from the top of the deposit and the various parameters of the sulphur deposit. These relationships allow the initial estimation of the deposit porosity, sulphur content and resource parameters.

Seismic imaging of the sulphurized carbonate rocks focuses mainly on the determination of porosity and related sulphur content. There is a strong correlation between deposit porosity and sulphur content, and the relationship of both these parameters with the amplitude of the reflection recorded from the top of the deposit [8]. On this basis, through changes in the amplitude of the reflection, it is possible to indicate:

- parts of the compacted deposit with increased sulphur content,
- privileged zones for process water flows,
- areas prospective for effective exploitation.

In turn, the structural image obtained from seismic surveys allows the determination of the position of the top and thickness of the deposit, as well as tectonic and facial disturbances.

However, the fundamental problem in seismic imaging of carbonate intervals is that they are characterised by high heterogeneity in the horizontal and vertical directions while, at the same time, by very high velocities. The long wavelengths associated with these velocities are usually unable to map their inner morphology, as high velocities in carbonates generally mean that seismic resolution is low [14,15]. Within the study area the thickness of the carbonate sequence is rather low, typically 10 and 30 m with a sulphur content in the range 0–30%. The properties of the deposit layer (porosity and sulphur content) show vertical and horizontal changes. Horizontal variability is particularly high, characterised by different degrees of consolidation of the carbonate layer, which causes lateral changes in porosity and sulphur content. For this reason, for the seismic imaging of such a specific case, the acquisition design and processing steps must be adjusted to obtain a high-resolution seismic image. Nevertheless, reflection seismic sections provide only qualitative information about the sulphur resources and are rarely used for quantitative evaluation of the distribution of petrophysical parameters within the reservoir rock. For quantitative interpretation, seismic inversion is used, which allows transformation of the seismic data from the amplitude domain to the impedance domain. The relationship between porosity and impedance allows quantitative interpretation of the parameters in carbonate rocks [16–19].

This paper presents the results of a high-resolution shallow seismic reflection survey that was acquired to identify a new area for sulphur exploitation to extend the Osiek sulphur mine. From many years of surveying within the area of sulphur deposits we have developed a special methodology for seismic acquisition and adopted the method of data processing, which is widely used in hydrocarbon seismic exploration, but rarely utilized in shallow seismic surveying. This allows us to obtain the relative amplitude preserved data necessary for reservoir characterisation [13,20–22]. To evaluate the deposit, we used and compared two methods of estimating the sulphur content. The first one is a novel method introduced by the authors which is based on calculating the porosity directly from the amplitude of the wave reflected from the top of the deposit. The second one is based on utilizing well logs and calculating seismic inversion, the result of which (acoustic impedance) was converted into porosity within the deposit. This is the standard method widely used for quantitative seismic reservoir characterisation. The porosity determined by both methods was converted into sulphur content using the correlation between these parameters, developed based on the analysis of numerous borehole logs from the study area. According to our knowledge, there has been no previous application of the seismic method

to assess the resources of shallow ore deposits directly from the amplitudes of reflected seismic waves from the top of the reservoir. The results of estimating the abundance of carbonate sulphur deposits are presented based on the example of a seismic cross-section from the Osiek sulphur mine. Our method allows indicating the most prospective zones suitable for exploitation.

2. Materials

2.1. Study Area

The study area is located in SE Poland, in the northern part of the Carpathian Foredeep (Figure 1a). The Carpathian Foredeep, within which the Polish biochemical deposits of native sulphur occur, forms a vast and elongated basin between the edge of the Carpathians and the edge of the Polish Uplands and the East European Platform [23]. The basin is filled with Miocene formations reaching a thickness of over 3000 m in the central part of the Foredeep. Depending on the region, the Miocene of the Carpathian Foredeep lies on Precambrian, Palaeozoic or Mesozoic formations. The variable morphology of the basement (numerous faults and uplifts) causes facial differentiation of the Miocene formations. The Miocene formations are overlain from the south by the Carpathian Flysch formations, and they are partly folded at the edge of the Carpathian overthrust [24,25].

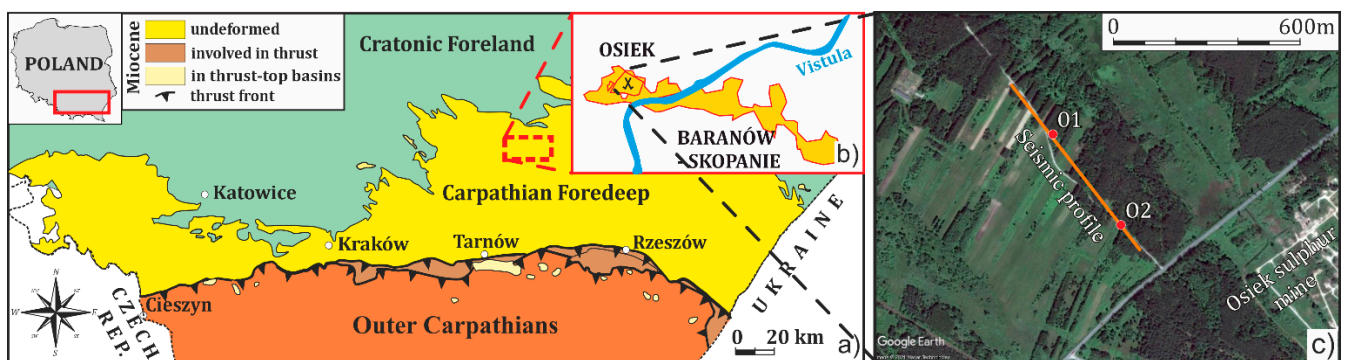


Figure 1. (a) Location of the study area (dashed rectangle) in the Polish Carpathian Foredeep; (b) Osiek sulphur deposit; (c) Location of seismic profile (orange line) and wellbores (red circles; source of map: Google Earth).

The Miocene formations include the Badenian and Sarmatian deposits [26]. The Badenian sediments are generally shallow-water sands, silts, limestones, marls and gypsum. In the northern part of the basin, they are up to 200–300 m thick. In the southern part their thickness is greater and rock salt appears among them. In the Sarmatian age, the strong subsidence of the central part of the Foredeep enabled the accumulation of siltstone, mudstone and silty sandstone [23].

In the area of occurrence of the deposits (Figure 1a) the Sarmatian sediments are referred to as Krakowiec clay deposits. Below them there are marly and silty pectenic layers (of a thickness of several to several dozen metres), classified as Badenian strata. Beneath them are gypsum-bearing formations, defined as the evaporite horizon (chemical series) or gypsum layers, with which the sulphur deposits are connected. The evaporite horizon is underlain by the sands, sandstones or siltstones of the Baranów beds and sometimes by algal limestones. These formations complete the profile of the Badenian deposits.

The Osiek deposit (Figure 1b) occurs in a belt about 2 km wide and 18 km long. The Vistula River divides the area of the deposit into two parts: left-bank (Osiek deposit) and right-bank (Baranów-Skopanie deposit). The thickness of the sulphur-bearing limestones ranges from several to several dozen metres, locally even up to 46 m, with an average thickness of about 21 m. The depth of the deposit varies from 100 m in the Osiecki region to 260 m in the Baranów-Skopanie section. Native sulphur is extracted using the Frash method, which involves injecting super-heated water into a sulphur deposit so that the sulphur melts and is pumped to the surface using compressed air.

2.2. Rock Properties of Sulphurized Carbonate Deposit

The investigation of the properties of the deposit layer, achieved by well logging, has provided very precise information on the variations of its properties, i.e., P-wave velocity (compressional velocity), bulk density, porosity, sulphur and clay content.

Based on the results of well logging, which document the deposit parameters, a relationship between porosity and sulphur content was determined using a broad data set from over 50 boreholes in the Osiek area (Figure 2). It can be observed that the porosity decreases with increasing sulphur content. This relationship is true in the 3–22% porosity range. Beyond the limits of this range, data abundance is small and the distribution of these parameters random.

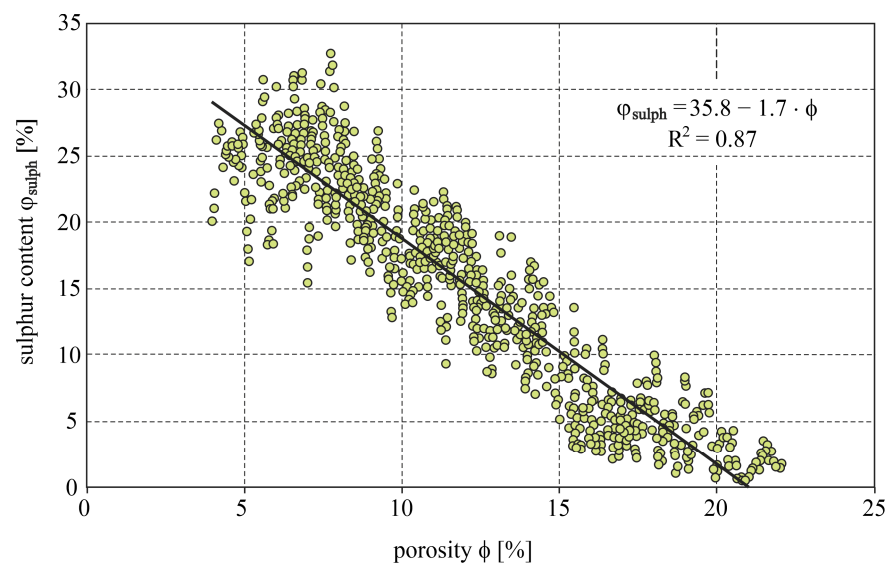


Figure 2. Empirical relationship between porosity and sulphur content within the carbonate deposit estimated from over 50 boreholes from the Osiek area [6,10].

This is a general relationship valid for the whole area of the deposit. The linear estimator for this relationship has the following form:

$$\varphi_{\text{sulph}} = 35.8 - 1.7\phi, \quad (1)$$

where: φ_{sulph} —sulphur content [%], ϕ —porosity [%].

The properties and composition of the deposit in the study area are shown in Figure 3. The deposit layer is characterised by a high P-wave velocity (approx. 4000 m/s) in relation to the overburden (1780 m/s). The deposit is dominated by a limestone skeleton, with an average clay content of a few percent.

The average P-wave velocity in crystalline sulphur is 2500 m/s [27], while in water it is 1410 m/s. The P-wave velocity for the limestone skeleton can reach up to 6200 m/s [28]. Due to the small presence of clay matter, the reservoir interval can be described by a three-component model (limestone, sulphur and porosity filled with water), in which case the value of the P-wave velocity can be calculated according to Wyllie's equation [29]:

$$\frac{1}{V_P} = \frac{1 - \phi - \varphi_{\text{sulph}}}{V_m} + \frac{\phi}{V_w} + \frac{\varphi_{\text{sulph}}}{V_{\text{sulph}}} \quad (2)$$

where: V_P —estimated P-wave velocity of the deposit layer, V_{sulph} —velocity of sulphur, V_w —velocity of water, V_m —velocity of limestone skeleton, ϕ —porosity, φ_{sulph} —percentage sulphur content.

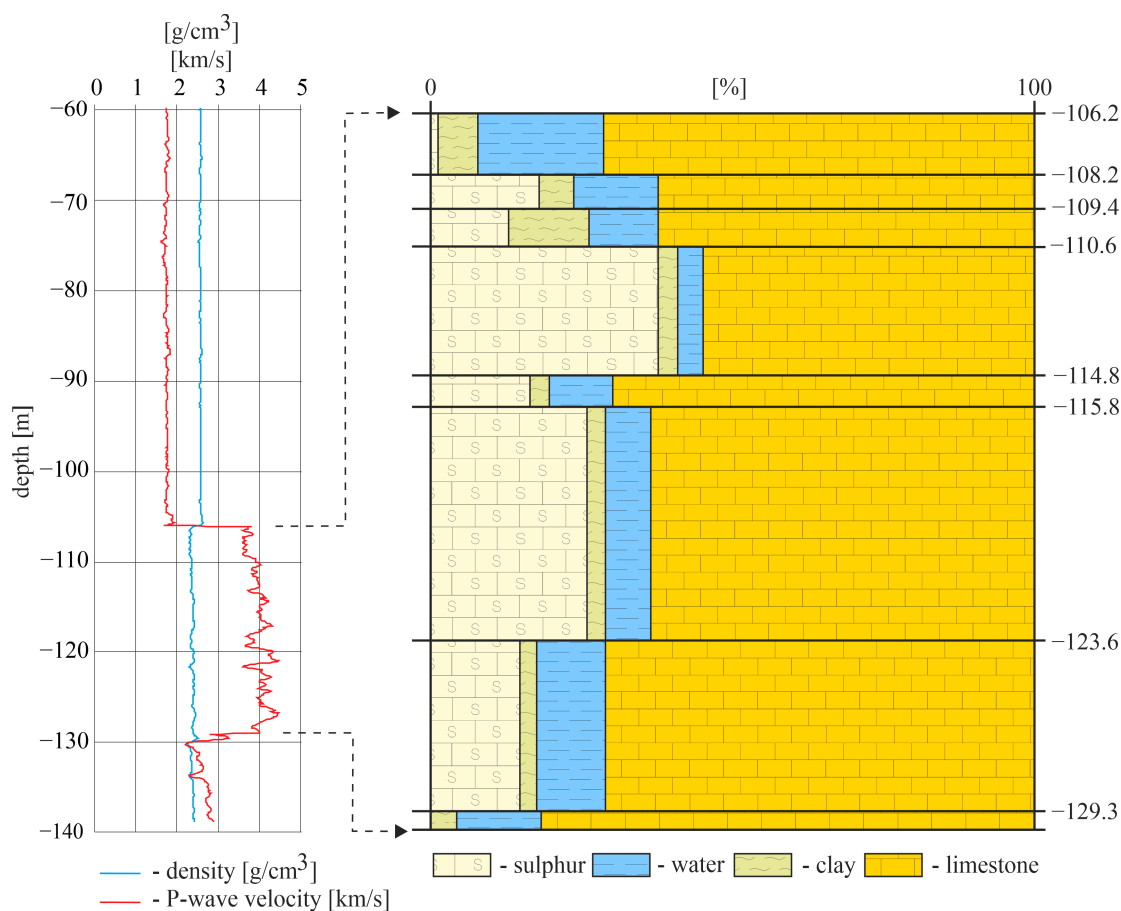


Figure 3. Wellbore O2. From the left: P-wave velocity (red log), bulk density (blue log) and lithology.

Inserting (1) and transforming Equation (2), we obtain the P-wave velocity function depending only on porosity:

$$\frac{1}{V_P} = \frac{1 - \phi - (0.358 - 1.73\phi)}{V_m} + \frac{\phi}{V_w} + \frac{(0.358 - 1.7\phi)}{V_{sulph}} \tag{3}$$

In Equation (3), the sulphur content is taken into account through a functional relationship, so the velocity depends only on the porosity. An estimator constructed in this form will approximate the average velocity value for a given porosity.

A change in porosity will induce a change in velocity with an accompanying change in sulphur content. The black line in Figure 4 represents the distribution of the P-wave velocity values determined by the estimator for the three-component model and the velocity value in the consolidated limestone skeleton of 6220 m/s. The black dots are the interval velocity values determined from well logging. The very good fit of the model values to the real data is evident. A significant decrease in velocity can be observed with increasing porosity of the reservoir rock (in the range 4000–3300 m/s). As we mentioned earlier, Equation (3) describes well the reservoir properties at low concentrations (several percent) of the clay material and in the porosity range 3–22%. However, as well logging data show, in zones with low sulphur concentration the crystalline and massive limestone changes into marly limestone. The P-wave velocity in the limestone skeleton is then reduced to values of about 4000 m/s, resulting in much lower velocity values in the deposit layer. After correction for the clay content of the limestone skeleton (20%), velocity changes occur in the range 3200–2800 m/s (blue line in Figure 4). This model also agrees with the actual values (blue points).

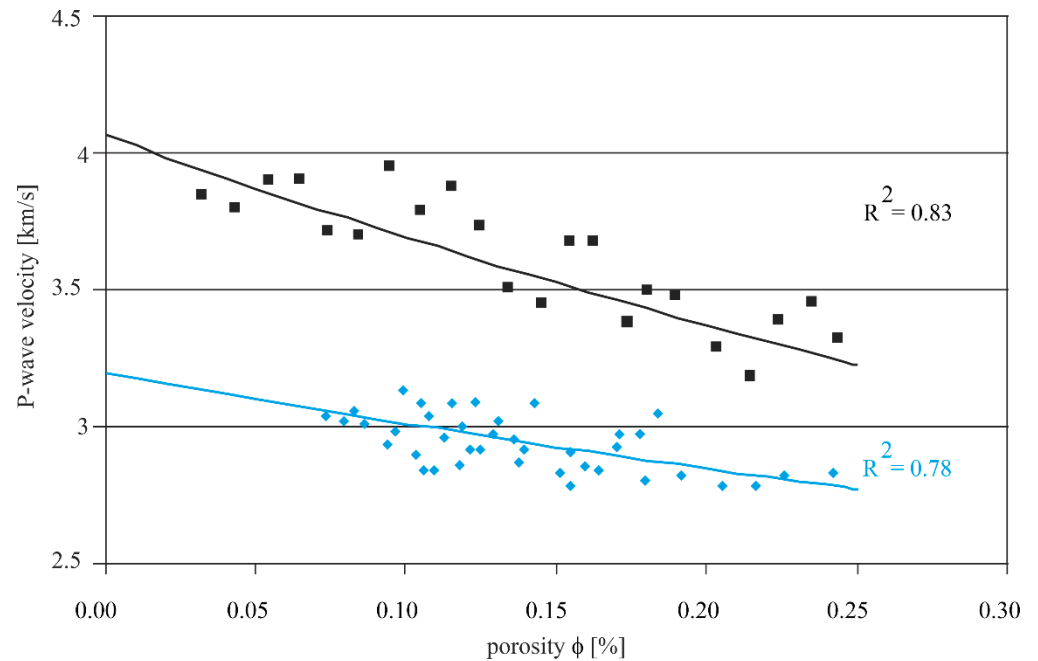


Figure 4. P-wave velocity as a function of porosity for the carbonate deposit calculated based on the Wyllie model. The black line represents the velocity estimator for massive limestone, and the blue line represents the velocity estimator for marly limestone. Both are overlaid with real values of velocity measured by well logging.

The distribution of sulphur content as a function of porosity, as shown in Figure 2, indicates that for a given porosity the deviation of sulphur content from the estimated value is about $\pm 7\%$. This results in a small error (2–3%) in the velocity values estimated according to Equation (3).

The presented velocity estimators show good correlation with the values found in the boreholes and clearly indicate that the change in porosity strongly influences the change in velocity and reflection coefficient (amplitude) values.

In addition to the velocity value, the reflection coefficient is significantly affected by changes in rock density, which is influenced by the rock's mineral content and porosity. For a two-component rock model (mineral frame and porosity), the relationship between bulk density and rock porosity can be described by Gardner et al. [30]:

$$\rho = \rho_f \phi + \rho_m (1 - \phi) \quad (4)$$

where: ρ —bulk density, ρ_f —density of the medium saturating the pore space, ρ_m —density of the rock skeleton, ϕ —porosity.

If we extend this relationship to the deposit layer model, the measured bulk density is the weighted sum of the densities of limestone, sulphur, clay and water (filling the pores of the rock):

$$\rho = \rho_w \phi + \rho_{\text{sulph}} \varphi_{\text{sulph}} + \rho_c \varphi_c + \rho_l (1 - \phi - \varphi_{\text{sulph}} - \varphi_c) \quad (5)$$

where: ρ —bulk density, ρ_w —density of the water, ϕ —porosity, ρ_s —density of the sulphur, φ_s —sulphur content, ρ_c —density of the clay, φ_c —clay content, ρ_l —density of the limestone.

The bulk density described by this relationship is related to all the components of the deposit layer: skeleton (calcite) with a value of 2.71 g/cm^3 , clay 2.4 g/cm^3 and sulphur 2.03 g/cm^3 [28]. For facial changes from crystalline massive limestone to marly limestone, the density decreases from 2.42 g/cm^3 to 2.23 g/cm^3 .

Based on P-wave velocity log in wellbore O2 (Figure 3), it can be observed that velocity contrasts within the reservoir are negligible, with an interval velocity of 3980 m/s . Similar values of interval velocities were also found in other wells. In general, the velocity values

vary from about 3200 m/s in highly porous zones with low sulphur concentration to about 4100 m/s in zones with strongly consolidated limestone and a sulphur content over 30%. The high velocity contrast between the deposit and the overburden (1780 m/s) results in a strong seismic wave reflection from the top and bottom of the deposit.

The analysis of the petrophysical properties of the sulphur deposits clearly shows that the value of P-wave velocity in the deposit and bulk density as well as acoustic impedance (product of P-wave velocity and bulk density) depend on porosity and degree of consolidation. The sulphur replaces water and thus reduces the porosity, which increases both P-wave velocity and bulk density. In fractured and porous zones, these values and the sulphur content will be low. On the contrary, in consolidated parts of the deposit, these values and the sulphur content will increase. It follows that the amplitude of the wave reflected from the top of the deposit will be strongly dependent on the porosity and thus on the sulphur content. This implies that areas of high sulphur content will appear as areas of strong amplitude.

3. Methods

The seismic reflection method is widely used in hydrocarbon [31] and mineral explorations [32,33]. It can reach up to several kilometers [34], registering frequency band spans comprising several tens of Hz with the dominant frequency typically below 40 Hz, which means that the imaging resolution is low, especially at greater depths. The shallow seismic reflection method differs from deep reflection method. It utilizes different energy sources, source-receiver geometries and a number of live channels. For example, the receiver spacing in deep seismic is in the range of 10–25 m with hundreds to thousands of receivers deployed, in the shallow seismic the receiver spacing is not greater than 5 m, with tens of receivers used for measurements. In contrast to deep seismic imaging, shallow seismic uses significantly lower energy sources (weight drops, sledgehammers) but with a much higher frequency range, guaranteeing higher resolution of data. However, higher frequencies are attenuated more rapidly than low frequencies limiting the depth range of investigation. Shallow reflection seismic method is commonly used in near-surface applications such as recognition of shallow geological structures [35,36], locating groundwater aquifers [37,38] and shallow exploration targets such as tin ore [39], coal beds [40–42] and gas deposits [43].

As mentioned earlier the seismic imaging of carbonate deposits require special care. The thickness of reservoir interval varies between 10 m and 30 m and carbonates are characterized by very high velocities. This means that the seismic resolution is low. In such a specific case, the acquisition design and data processing sequence must be adjusted to obtain a high-resolution seismic image.

Well logging is a set of borehole investigation methods that are based on special logging tools. It allows obtaining a continuous record of a formation's rock properties [44]. Interpretation of acquired well logs, such as resistivity, natural gamma, gamma-gamma, neutron porosity and sonic enables the determination of porosity, fluid saturation and lithology, i.e., mineral composition of formation [45]. Compared with the seismic method, the resolution of well logs is very high (tens of centimetres). Furthermore, well data is the key to correct petrophysical interpretation of the surface seismic data.

In the area of Osiek sulphur mine the standard set of properties from well logging data is available which comprises velocity, bulk density, porosity and lithology including the sulphur content.

3.1. Synthetic Seismic Response from the Deposit

When an incident P-wave strikes the interface between two media, the wave is split into reflected and refracted P-wave components and reflected and refracted S-wave (shear wave) components. The reflection and transmission coefficients vary as a function of the angle of incidence and the media's elastic properties such as seismic velocities and densities. The variations in reflection amplitude observed as a function of the angle of incidence can

be used to make inferences about the elastic parameters of the subsurface rocks. However, at angles of incidence larger than a critical angle, a critical reflection may occur, which cause significant distortion in amplitudes and rotation of the reflection phase. Such changes in a reflection are not related to the rock properties but only to the way the seismic wave propagates. The appearance of the critical angle depends on the depth of the interface and the contrast of elastic parameters and is described by Snell's law [46].

In the study region, the deposit top is a strong reflecting boundary with a very large positive reflection coefficient which, for a normal angle of incidence, reaches a value of 0.4. The high impedance contrast and shallow depth of the sulphur deposit (about 100–140 m) mean that for relatively small offsets (distances between the shot point and the receiver), a rapid appearance of a critical angle is observed. This phenomenon causes a significant reduction in useful offsets, for which there are no changes of amplitude and phase of the reflected signal. To determine the correct reflection amplitude—porosity relationship, the recorded seismic wavelet amplitude must not be affected by variations resulting from reflections in the vicinity of the critical angle. Additionally, to obtain a high signal resolution, amplitudes with a variable phase shift cannot be stacked within the common mid-point (CMP), as this underestimates the amplitude of the stacked signal and also changes its signature. To optimise the seismic acquisition and avoid the recording of redundant data we perform modelling to determine appropriate acquisition parameters.

The dependence of the reflected signal amplitude on the angle of incidence is described by the Zoeppritz equations [47]. A significant increase in velocity at the boundary at the top of the sulphur-bearing limestone layer causes the critical angle to be smaller or close to 30° and results in the signal amplitude value to increase rapidly for relatively small offsets. For angles larger than the critical angle the phase of the signal is rotated. A detailed discussion of the quantitative dependence for such a case is presented by Aki and Richards [46]. For a velocity model corresponding to reservoir conditions, i.e., average velocity contrast between overburden and limestone (1780/3600 m/s) and the depth of the interface equal 120 m, the change in signal amplitude and phase are shown in Figure 5a. The Zoeppritz Explorer Applet [48] was used for the calculations and assumed a P-wave and S-wave velocity ratio of 1.8 in both layers, and a bulk density for the overburden and limestone of 2.57 g/cm^3 and 2.37 g/cm^3 , respectively.

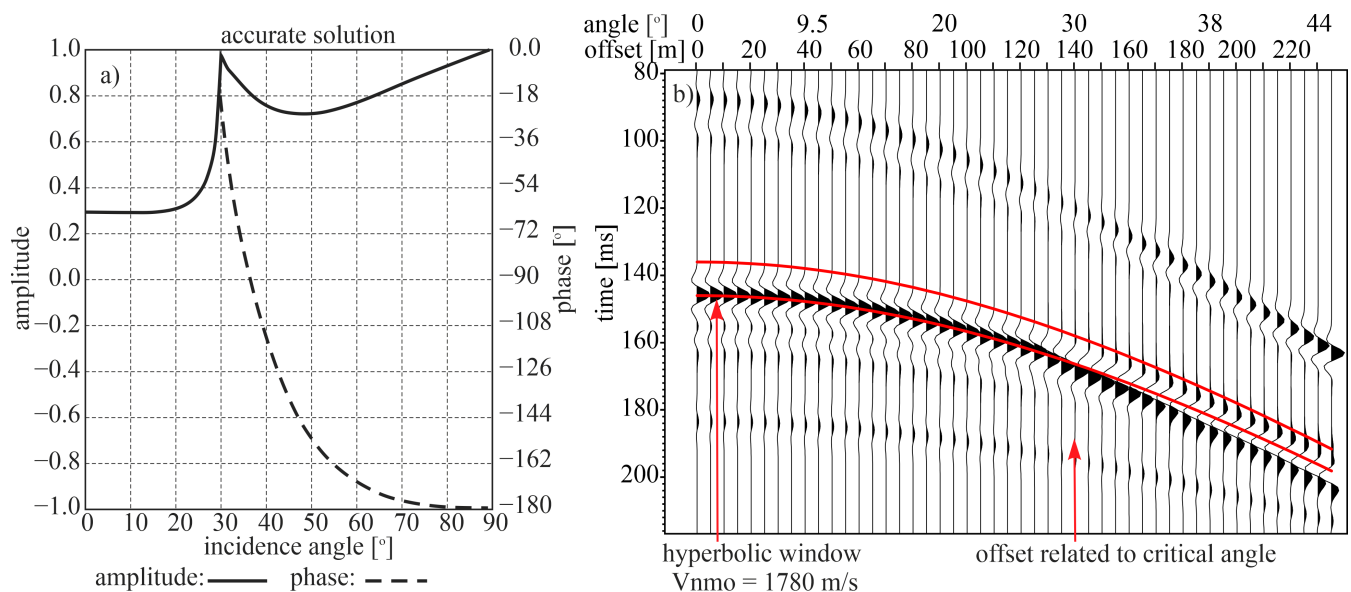


Figure 5. Synthetic seismic response from the carbonate sulphur deposit. (a) Change of reflection amplitude and phase of signal as a function of incident angle—accurate solution; (b) synthetic CMP gather.

For the deposit model, we also modelled the reflected wavefield in the CMP gather (Figure 5b). In the model, we assumed a layer thickness of 25 m, a layer top depth of 120 m, velocity in the overburden of 1780 m/s and the deposit of 3600 m/s, and a Ricker 90 Hz signal as the wavelet. The assumed layer velocity values for the overburden and deposit also correspond to values often determined from velocity analyses on field data. The modelling was carried out for an array length of 235 m, for which the receivers were located every 5 m. To illustrate the amplitude changes, the traces were normalised to the maximum amplitude value in the CMP gather. Figure 5b clearly shows a strong change in signal shape with offset. The effect of phase rotation is visible above the critical angle (30°). For the assumed model this angle corresponds to an offset of about 140 m.

For offsets close to the critical angle (110–140 m) there is a clear increase in the amplitude, and for an offset of 175 m corresponding to an incidence angle of 35° there is a 90° rotation of the signal (Figure 5b). The visible hyperbolic window (red) for the normal move-out velocity (V_{NMO}) of 1780 m/s shows that if we were to stack the signals there would be a distortion in the form and amplitude of the stacked signal.

Figure 6 shows the effect of stacking signals within the CMP gather (after NMO correction) for different offset ranges on the amplitude of the wave reflected from the deposit. For stacking, we used the synthetic CMP gather shown in Figure 5b. The result of stacking the synthetic CMP gather shows that in the offset ranges 0–115 m, 0–155 m and 40–155 m the amplitudes had similar values (in the range 4.2–4.4). However, stacking for all offsets (0–235 m) resulted in a clear reduction of the amplitude value to 3.2.

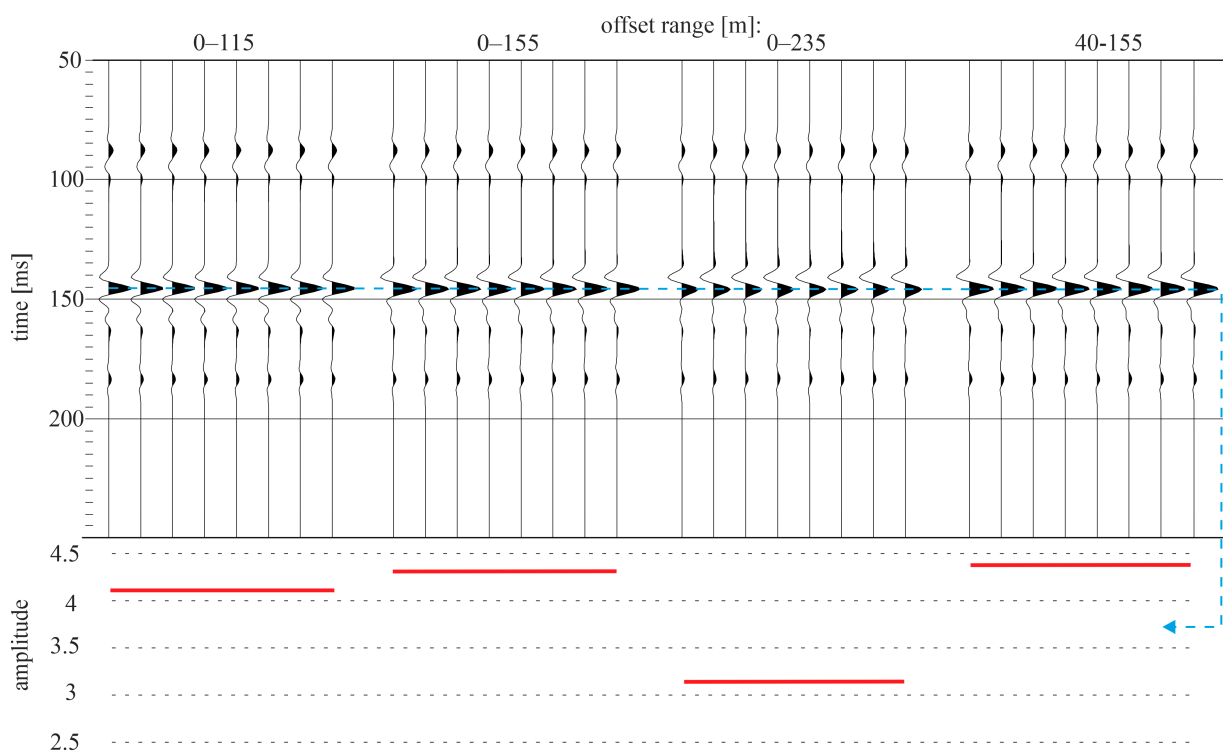


Figure 6. The effect of different offset ranges on the results for the stacking traces within a single CMP. The stacked CMP trace was duplicated 8 times for better presentation. (**upper**) From the left: stacking in the offset ranges 0–115 m, 0–155 m, 0–235 m, 40–155 m; (**lower**) amplitude of the reflection from the top of the deposit.

Similarly, to the synthetic data, for the field data we performed stacking for the offset ranges 40–155 m and 40–235 m (Figure 7a,b, respectively). The resulting cross sections were almost identical, differing only in details. However, in the values of amplitude of reflection from the deposit there were clear differences (Figure 7c). Increasing the offset value resulted in a decrease in the amplitude. This was especially true in the CMP 20–60 range, where

the interval velocity value was increased in the deposit and the top was slightly elevated. A local increase in velocity caused a decrease in the value of the critical angle, and the decrease in depth decreased the value of the offset corresponding to this angle.

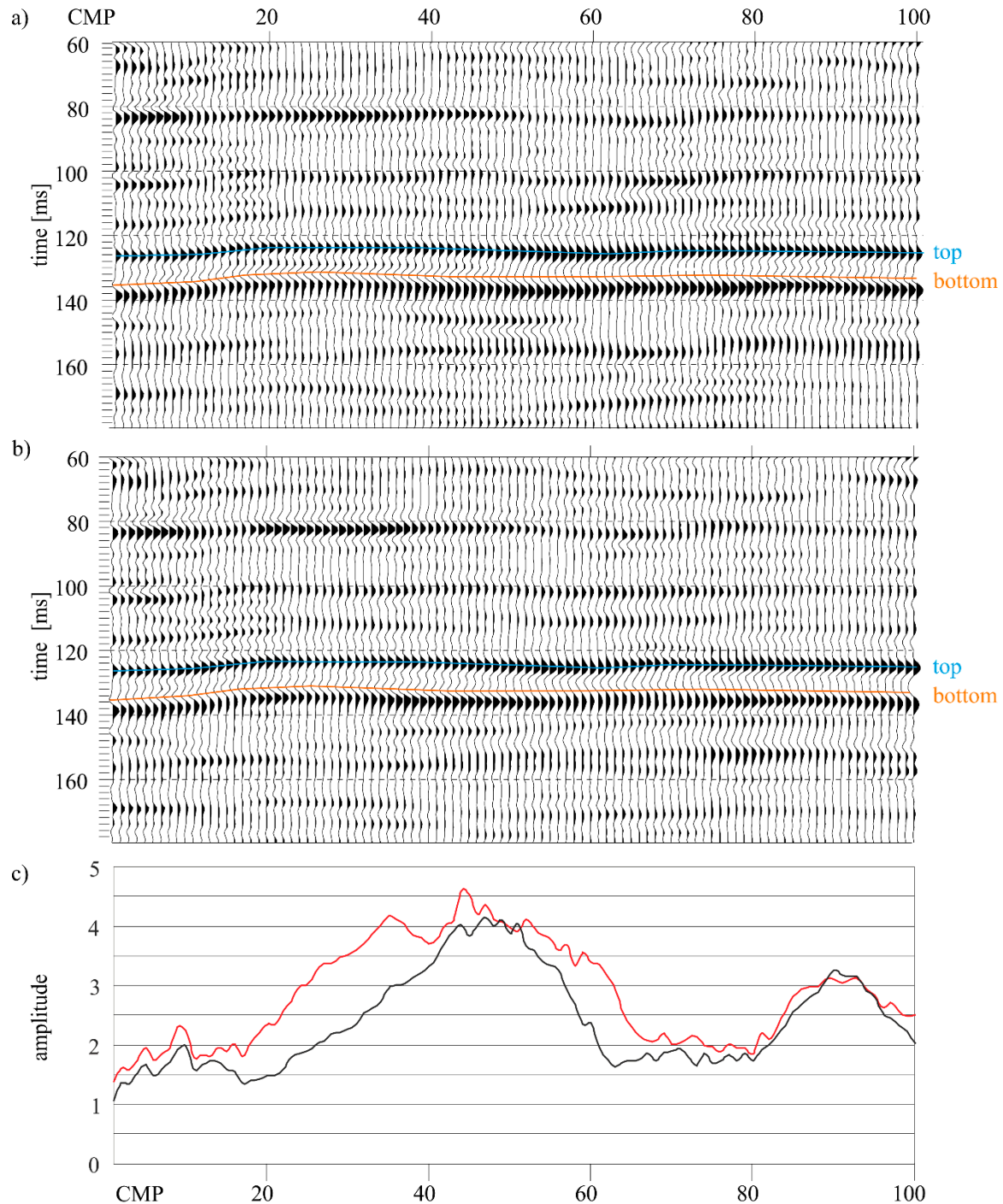


Figure 7. Fragment of a real seismic cross section showing the top and the bottom of sulphur deposit acquired by stacking different offset ranges. (a) 40–155 m offset range; (b) 40–235 m offset range; (c) graph of amplitude reflected from the top of the deposit, where the red line corresponds to offsets of 40–155 m and black line to offsets of 40–235 m.

The performed analyses suggest that to avoid unfavourable effects (increase in amplitude near the critical angle and phase rotation for larger angles) affecting the signal amplitude after the seismic stack, the range of incidence angles should be limited to about 25–28° during field measurements.

3.2. Seismic Data Acquisition and Processing

For seismic imaging of the shallow subsurface structures, it is crucial to design appropriate acquisition and processing parameters towards the given geological target [20]. In addition, if seismic surveys are performed for reservoir characterisation purposes, it is of utmost importance to maintain the true amplitudes during processing [13], as the values of signal amplitudes are directly related to the distribution of reflection coefficients, which depend on the petrophysical parameters of the rocks. The variation in the petrophysical parameters of the rocks will therefore be manifested on the seismic sections as vertical and horizontal changes in the amplitudes. In our case, the geological target (carbonate sulphur deposit) was located at a shallow depth of 100–140 m. The results obtained from modelling and analyses carried out on the measured data indicate the limitation of the range of incidence angles to about 25–28° during field measurements. This corresponded to limiting the offsets to about 155 m. This was a compromise value minimising the discussed distorting effects and at the same time allowing the use of 24 acquisition points with a measurement step of 5 m (and moving the shot point 40 m away to limit the occurrence of surface waves disturbing close offsets). This method of acquisition enables satisfactory data quality to be obtained.

Seismic data were collected using a Geometrics Geode recording system with 100 Hz vertical geophones (receivers) placed 5 m apart. 100 Hz geophones allow higher resolution to be achieved than with commonly used 10–24 Hz geophones because they perform better in the high frequency range and the same time better attenuate unwanted low frequency noise [49]. We used end-on roll-along spread with Gisco ESS-500 Turbo seismic source (accelerated weight drop of 227 kg—impact velocity of 6 m/s with an energy of 4088 J). The shot and receiver interval was 5 m. To obtain high signal to noise ratio at each shot position, typically three weight drops were performed. Then the corresponding records were vertically stacked. In places where the ground was loose then more than three drops were performed. By performing acquisition in the 40–155 m offset range, coherent noises such as surface wave and air wave occur at times greater than the reflections from the top and bottom of the deposit. In such a case, the amplitudes of these waves do not disturb the response from geological target and do not have to be cut out at the processing step. The use of filters to remove such interference usually leads to a distortion of the signal amplitude. The designed geometry allowed us to obtain an average fold of about 12 with a CMP spacing of 2.5 m. Table 1 summarizes the main acquisition parameters used to acquire the data. Figure 8 shows one of the acquired raw shot record. The acquired seismic data have good quality overall, with clear reflections from the top and bottom of the carbonate sulphur deposit.

Table 1. Seismic acquisition parameters.

Feature	Measurement
Source type	Gisco ESS-500 Turbo (accelerated weight drop)
Recording system	Geometrics Geode
Receiver	Single vertical 100 Hz geophone per channel
#Active channels	24
Vertical stacks	3 times average, max up to 10
Receiver interval	5 m
Shot interval	5 m
CMP interval	2.5 m
Absolute offset range	40–155 m
Average fold	12
Sampling rate	0.5 ms
Record length	512 ms
Profile length	625 m

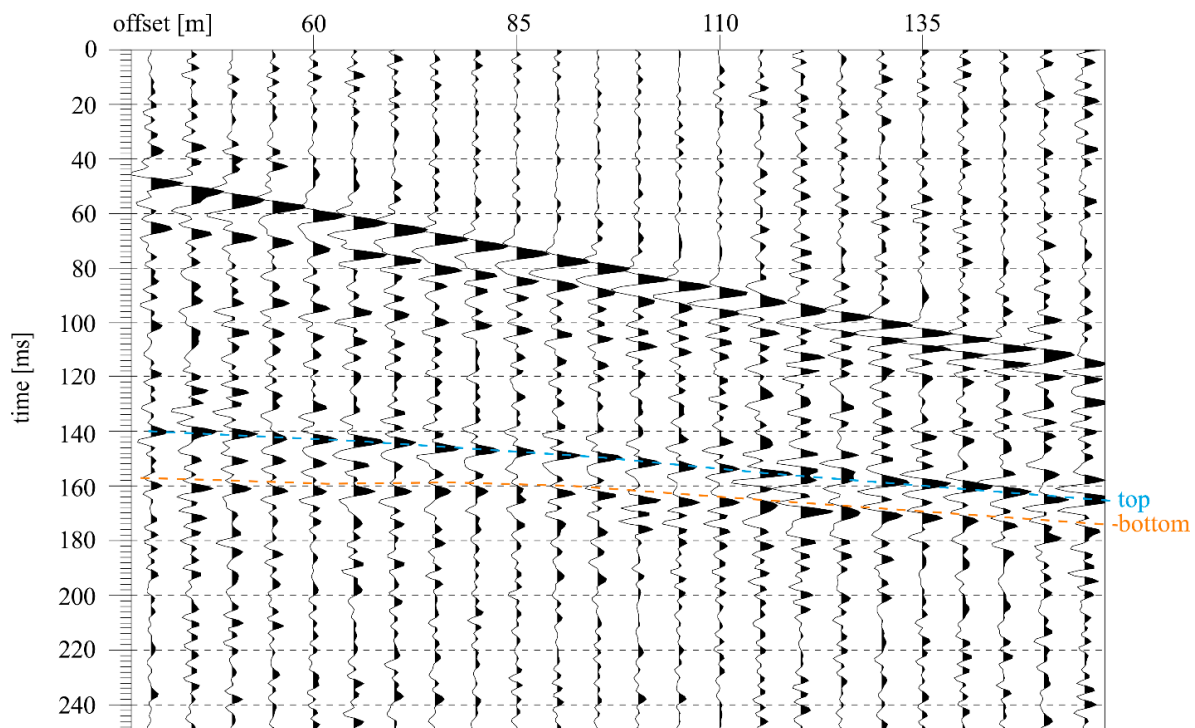


Figure 8. Exemplary shot record after trace normalization (for display purposes only). Due to the high quality of the acquired data, reflections from top and bottom of the deposit can be unequivocally identified. They occur at 140 and 160 ms, respectively, and are characterized by high amplitudes compared to other reflections.

The acquired data were processed with relative amplitude preservation (RAP), which is necessary when we want to use seismic for quantitative reservoir characterisation, e.g., using inversion [13,21,22]. However, compared with hydrocarbon seismic exploration, this methodology of data processing is rarely utilized for shallow reflection seismic profiling [20] where limited acquisition parameters are used (low number of channels). RAP processing means that no invasive methods of signal enhancement can be applied and noise has to be filtered only with extreme caution. We have to be sure that no signal is removed during the filtering. In addition, no harsh amplitude scaling can be applied, as it significantly disturbs the relative amplitudes. The main problem in seismic data processing is how to suppress the surface wave (which is the strongest noise on seismic records) without affecting the signal that lies underneath it. Since we designed and applied a tailored acquisition, the surface wave was not much a concern in our case, as it occurred below a geological target and did not interfere with it. This meant we were able to maintain undisturbed amplitudes of the reflections from both the top and bottom of the carbonate reservoir.

Data were processed using Vista 2D/3D Seismic Data Processing software (version 2020). The applied processing sequence is presented in Table 2. Pre-processing included geometry application and removal of noisy channels that resulted from poor geophone coupling. Due to a gradual loss of amplitude, a result of wavefield geometric divergence, we applied a correction that compensated for this unwanted effect. For the shallow seismic boundaries and long offsets, the loss of energy was substantial. Therefore, in addition to applying the standard time correction, we also included an offset component in the calculation. For coherent noise removal, such as the surface and air waves, the Radial Transform was applied [50]. This procedure requires the generation of a surface wave model, which is then removed from the real data. The surface wave model was generated with apparent velocities of up to 350 m/s. An adaptive filter was designed to fit the model traces to the real traces and then, in the time domain, the filter was applied to the model traces and subtracted from the real traces. After this procedure we compared the inputs and outputs to ensure that the useful signal had not been removed and the amplitudes were

undamaged. For reservoir characterisation, in RAP processing the variations in amplitude of seismic reflections should only be caused by variations in the petrophysical parameters of the subsurface. However, variations in the amplitude phase or frequency depends also on changes in the source and receiver conditions (e.g., a seismic wave generated on hard ground will give different amplitudes than on soft ground). To compensate for these effects, we use surface-consistent methods [51]. In surface-consistent amplitude scaling, we compensate for the effect of amplitude variations caused by different shot point conditions and poor geophone coupling. The surface-consistent spiking deconvolution was used to improve vertical resolution and balance the amplitude spectra. After deconvolution we applied a 40/60–200/250 Hz bandpass filter for attenuation of the high frequency noise that was provided by the deconvolution and to attenuate the residues of the surface waves that were not completely removed by the Radial transform. In the next step the seismic data were moved to floating datum, which was set to smooth ground elevation. Then we perform standard procedures of refraction statics, velocity analysis and normal move out corrections (NMO) and stack. Finally, the stacked seismic data were migrated with the Kirchhoff algorithm using a smoothed version of the stacking velocities. The obtained seismic cross section (Figure 9) has a high signal to noise ratio and dominant frequency of approx. 90 Hz. Assuming P-wave velocity in deposit of approx. 4000 m/s, the obtained seismic resolution is about 11 m, which in our case is considered as a high and satisfactory result.

Table 2. Seismic data processing sequence.

Procedure
Geometry and trace edit
Geometric divergence correction (offset-dependent)
Noise removal with signal preservation
Surface-Consistent Amplitude Scaling (source and receiver)
Surface-Consistent Spike Deconvolution (source and receiver)
Bandpass filtering (40/60–200/250 Hz)
Datum (floating), refraction statics
First break muting
Velocity analysis
NMO
Automatic residual statics
Stack
Post-stack Kirchhoff migration

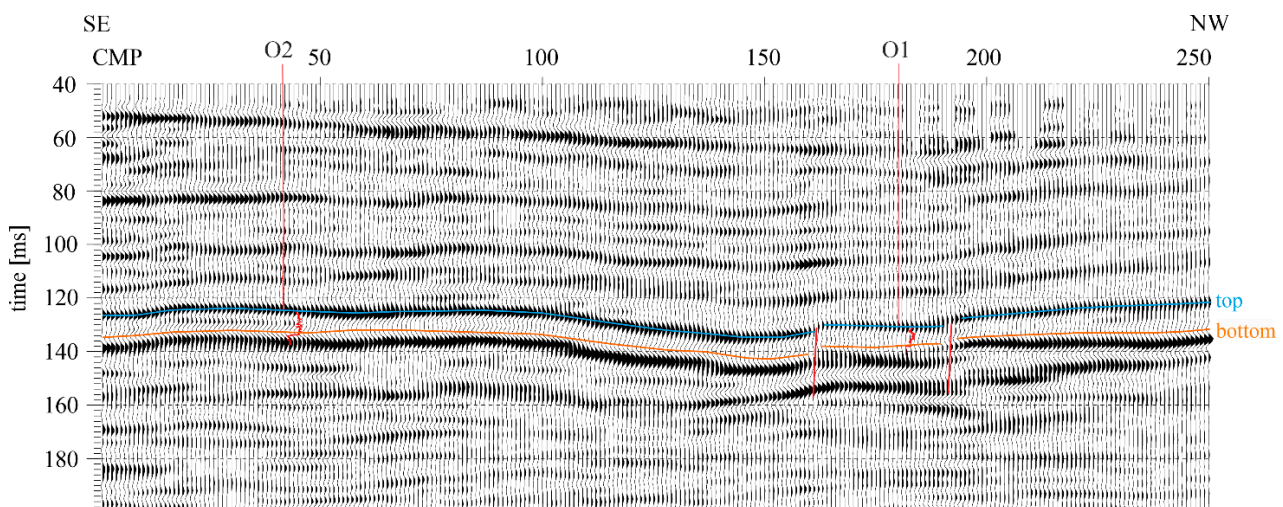


Figure 9. Seismic cross section with interpretation and boreholes with P-wave velocity logs displayed. Blue and orange horizons show top and bottom of the deposit respectively.

4. Results and Discussion

4.1. Estimation of Sulphur Reserves

As confirmed by our studies, seismic surveys make it possible to establish the quantitative relationships between the amplitude of the seismic signal recorded from the top of the deposit and its petrophysical parameters. First, we have to calculate an RMS (the root mean square) amplitude, which is determined in a narrow window whose centre coincides with the position of the top boundary. Then the calculated amplitudes are calibrated to the value of the reflection coefficient from the deposit, which in turn is calculated based on data from boreholes located in the vicinity of the analysed profile. Scaling of signal amplitude “A” recorded at a given point “x” of the seismic profile to the value of reflection coefficient r is performed according to the following equation:

$$r(x) = \frac{A(x)r_{\text{well}}}{A(x_{\text{well}})} \quad (6)$$

where: $A(x_{\text{well}})$ —amplitude from the deposit recorded at the position of borehole, r_{well} —value of the reflection coefficient from the deposit at the position of borehole.

The reflection coefficients obtained in that manner correlate very well with the average porosity values determined from the borehole data (Figure 10). The relationship between average porosity and reflection coefficients (r) can be estimated by a linear equation:

$$\phi = -29.829r + 21.988 \quad (7)$$

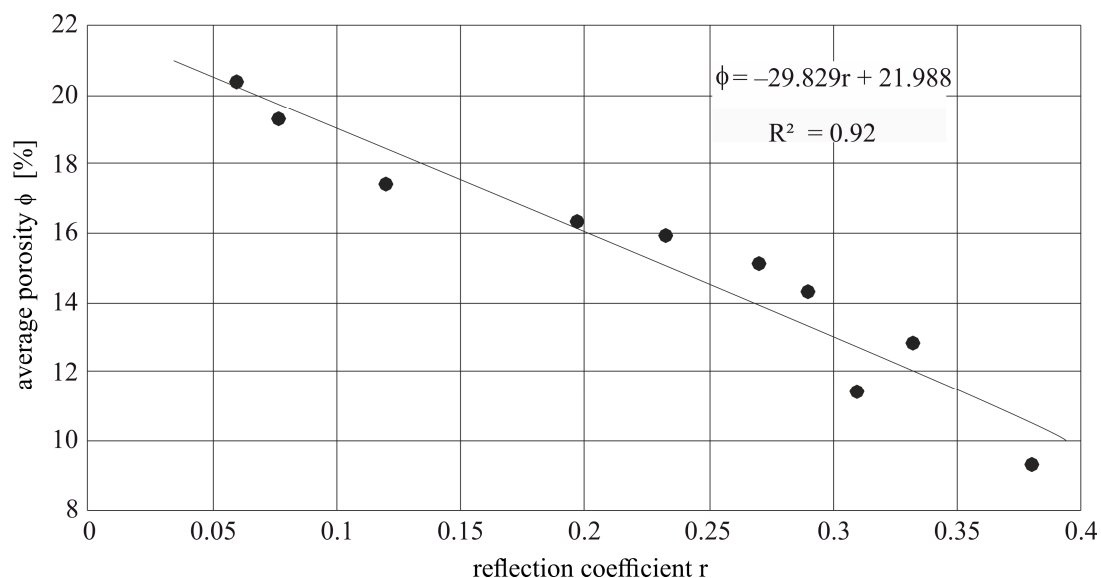


Figure 10. Relationship between average porosity calculated from several boreholes and reflection coefficients from the top of carbonate deposit at their location.

Finally, by inserting Equation (7) into Equation (1), the porosity of the carbonate deposit can be converted into sulphur content.

In the case of intersecting profiles, they should be scaled so that in points of mutual intersection of the profiles the values of amplitudes are equal. Then, based on relationship (6), the signal amplitudes are scaled along all profiles. In this way an intersecting profile, which is not located near any borehole, can also be scaled to the reflectivity value.

Based on the established relationships we performed an analysis of the seismic profile. Figure 11 shows the interpreted seismic cross section. Between CMP 160 and 190 there is a zone of tectonic disturbance in the deposit. Remnants of diffraction waves that were not removed in the migration process are visible. These cause distortions in the amplitude of the deposit top reflection. For this profile, after calculating the deposit reflection coefficient

according to Equation (6) using estimator (7), we were able to calculate an approximate value of the average porosity of the deposit (Figure 11c—black line).

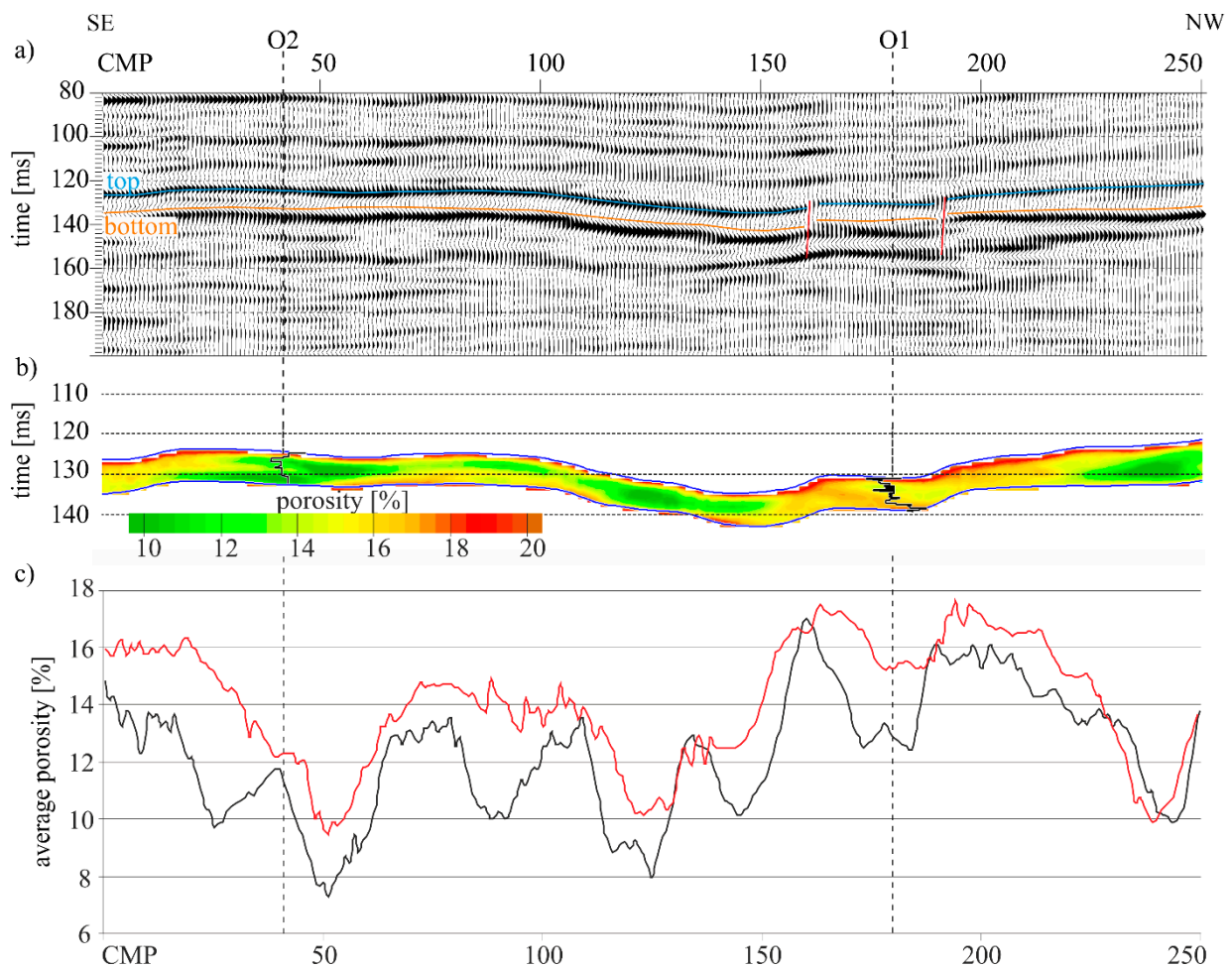


Figure 11. (a) Seismic cross section (see Figure 9 for description); (b) spatial distribution of porosity within the deposit derived from seismic inversion, with porosity logs displayed; (c) diagrams showing calculated porosity: red line—average porosity from seismic inversion, black line—porosity from amplitude of reflection from the top of deposit.

We wanted to compare our method of calculating porosity with the standard procedure that is used for seismic reservoir characterisation—seismic inversion. This method utilizes seismic and borehole data to transform the seismic data from the amplitude domain to the impedance domain, which gives insight into the quantitative petrophysical parameters of the subsurface [52,53]. Seismic inversion was calculated using Hampson-Russell software (version 10). For the calculation of impedance, Post-Stack Model-Based Inversion was used [54]. In this method, a simple model of the subsurface is designed through the interpolation of well log measurements (P-wave velocity and bulk density) along interpreted horizons and then recursively altered until the derived synthetic section best fits the original seismic data. Then using a derived relationship between porosity and acoustic impedance (Figure 12), we transformed the result of the inversion into the spatial distribution of porosity. Figure 11b shows the porosity distribution in the reservoir correlated with borehole data. For the porosity distribution obtained in this way, the value of average porosity within the deposit was calculated for each CMP (Figure 11c—red line).

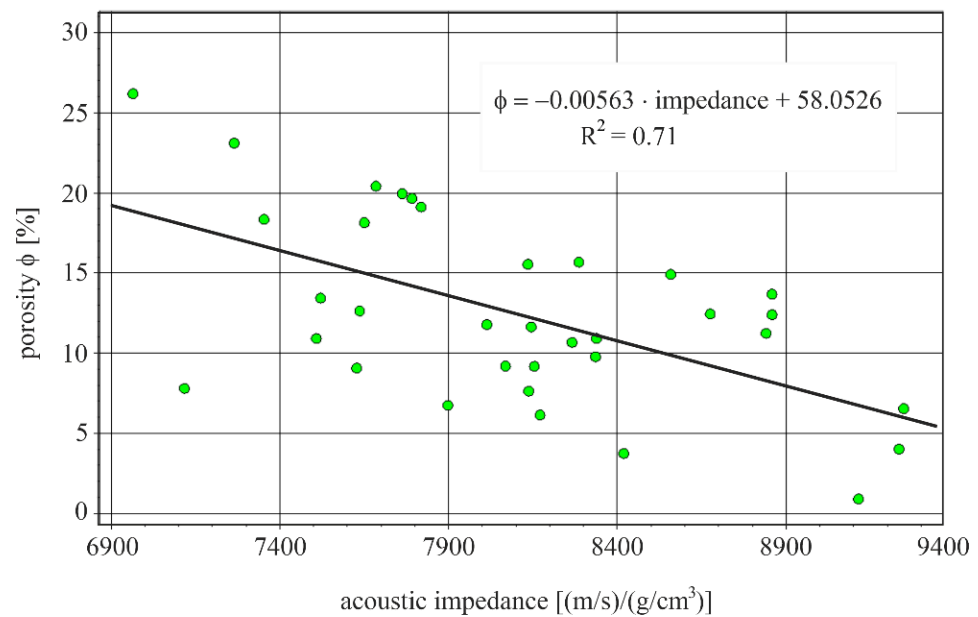


Figure 12. Relationship between porosity and acoustic impedance for wellbore O2.

The porosity distributions determined from both methods along the analysed profile are similar to each other (Figure 11c). In addition, they are comparable with the porosity distribution obtained from well logging (curves displayed in Figure 11b). Absolute differences of up to 4% can be observed between CMP 20–30 and 170–190. A particularly large difference occurs in the surroundings of CMP 180 and this is most probably due to the change in the values of amplitudes in a tectonically disturbed zone.

Finally, we calculated the sulphur content for both porosity estimation methods using Equation (1). The percentage of sulphur content determined from seismic inversion is on average a few percent lower than for the method based directly on calculation from the amplitude of the wave reflected from the top of the deposit (Figure 13). Excluding the surroundings of CMP 180, where tectonic disturbances occur, the differences were not large and the general trends were similar.

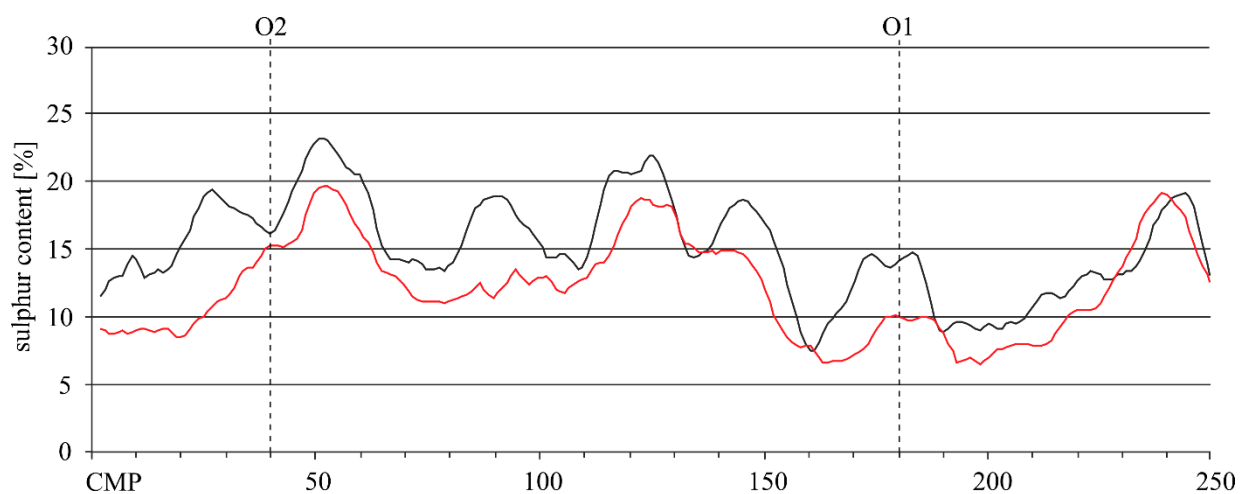


Figure 13. Comparison of sulphur content calculated using both methods along the analyzed seismic cross section. Red line—sulphur calculated from seismic inversion, black line—sulphur calculated from amplitude from the top of the deposit. Both graphs were smoothed with a running average of 3 CMP.

A summary of the average deposit parameters measured in the boreholes and calculated from the values of amplitude of reflection from the deposit top and by the inversion method is presented in Table 3. The average porosity value in borehole O2 was 11.9% and in borehole O1 was 12.4%. The porosity values estimated from the inversion were 12.1% and 15.1%. In contrast, the porosity values determined from the amplitude of the top of deposit were 11.6% and 12.7%, respectively. This suggests that the calculations of porosity directly from amplitudes give more realistic results than from seismic inversion.

Table 3. Comparison of derived average petrophysical parameters from well logs, amplitudes from the top of deposit and seismic inversion.

Parameter	Borehole Measurement	Derived from Amplitudes	Derived from Inversion
Porosity (%)	11.8 (O2)	11.6	12.1
	12.4 (O1)	12.7	15.1
Sulphur (%)	16.0 (O2)	16.1	15.2
	13.8 (O1)	14.2	10.1

Similarly, the true average sulphur content of 16% and 13.8%, respectively, is better estimated for the porosity calculated from the amplitude of the reflection. This method yielded values of 16.1% and 14.2%. Calculations from the seismic inversion slightly overestimated the porosity values and thus lowered the sulphur content by about 3% on average. Nevertheless, the area between CMP 20 and 150 and the surroundings of CMP 240 can be indicated as the most prospective zones and are suitable for exploitation as they are characterized by low porosity hence high sulphur content.

4.2. Discussion of the Results

The main aim of our study was to estimate the sulphur content from the shallow carbonate deposit that occur at depths of 100–140 m and are approximately 25 m thick. For this, we performed high-resolution shallow seismic reflection profiling. Since the survey was intended to perform a quantitative estimation of the shallow sulphur deposit, we designed and applied tailored acquisition scheme and processing sequence. This, along with the application of well logs, allowed us to obtain a realistic distribution of the sulphur content within the carbonate deposit and allow for planning of the location of new boreholes. The results of research to date, verified by drilling, indicate that the absolute error in sulphur calculation is small. The areas mineable for sulphur are characterized by relatively low porosity hence high sulphur content.

Our method of evaluating sulphur from the amplitudes reflected from the top of the deposit gives smaller errors in the calculations than by utilizing seismic inversion. This is most probably caused by the relatively low resolution of the seismic record in relation to the resolution of well logging data. The thickness of the deposit along analysed seismic cross section varies in the range 20–25 m. For a dominant wavelet frequency of approx. 90 Hz and P-wave velocity in deposit of approx. 4000 m/s, the seismic resolution is about 11 m. At such a resolution, the presence of thin layers (several dozen centimetres) of increased porosity within the deposit results in the overestimation of this value while using seismic inversion. In addition, acoustic impedance is not solely related to changes in the porosity as it can be affected by many other factors. Therefore, the vertical and horizontal changes in acoustic impedance within the reservoir may also be related to facial changes, uneven sedimentation, hydrocarbon saturation or organic matter content [55]. This means that the acoustic impedance alone is not the most suitable tool for reservoir characterisation within carbonate rocks. Some authors suggest using a seismically derived Lamè constant and shear modulus [56,57]. These parameters are more sensitive to porosity and lithology changes and thus enable more precise reasoning than for acoustic impedance. However, this requires estimating both the acoustic and shear impedances from seismic data by

performing a simultaneous inversion [58]. Simultaneous inversion, compared to post-stack inversion, utilizes pre-stack data (CMP gathers) to determine the acoustic and shear impedance volumes. However, this method is more demanding as it requires high fold, long offsets and S-wave measurement in the boreholes. We perform simultaneous inversion in the area of the Basznia sulphur mine, which allows us to distinguish zones of reduced porosity (higher sulphur content) from zones associated with lithofacial changes [13].

In the Basznia sulphur mine, the carbonate formations lie at a depth of approximately 250 m while the deposit itself is consolidated, with a high sulphur content. The horizontal and vertical variability of the petrophysical parameters is not significant. In contrast to the Basznia deposit, the sulphur deposit at Osiek occurs much shallower. The top of the deposit lies at depths of about 100 m to about 140 m. The thickness of the deposit varies from 10 to 30 m and the sulphur content from 0 to 30%. The properties of the deposit layer (porosity and sulphur content) show vertical and horizontal variability. The horizontal variability is particularly high, characterised by different degrees of consolidation of the limestone layer, which causes lateral changes in the porosity and sulphur content. In this case, for quick initial recognition of changes in its properties, we proposed a method of estimating porosity and sulphur content based on the amplitude of reflection from the top of the deposit. This allows a satisfactory recognition of prospective zones as well as delimitation of zones with low sulphur concentrations.

We believe that the presented method can be successfully applied for imaging other deposits when a strong relationship exists between amplitude and the petrophysical parameter we are interested in. Especially in situations, where standard seismic inversion cannot be used (lack of velocity or density well logs). Currently, we are trying to incorporate the spectral decomposition to investigate facial changes within carbonate deposit. The spectral decomposition allows mapping the objects of thicknesses below the seismic resolution [59]. This would aid recognition of the changes occurring within the rocks and thus distinguish between the effects of facial and porosity changes on the acoustic impedance. Such a method would further reduce miscalculation of sulphur content and other petrophysical parameters, especially at sites where simultaneous inversion cannot be applied.

5. Conclusions

In this article, we have presented the application of the high-resolution seismic survey for estimation of shallow sulphur deposit resources. For this we developed a method of seismic acquisition and processing that allows us to estimate the sulphur content directly from the amplitudes of reflected seismic waves from the top of the deposit. Then, we compared our method with the standard method that is commonly used for reservoir characterisation—seismic inversion. Some conclusions are worth noting:

- (1) Seismic reflection surveys make it possible to initially identify a shallow sulphur deposit, delineating zones with higher sulphur content, and plan a location of new boreholes.
- (2) The increase in sulphur content within the deposit is accompanied by a decrease in porosity due the sulphur filling the pores. With the higher sulphur mineralization, the rock matrix is stiffer.
- (3) A decrease in the porosity causes an increase in the amplitude of the seismic signal reflected from the top of the deposit. The areas with low porosity (high sulphur content) will be manifest at seismic cross sections as areas of strong amplitudes.
- (4) Recognition of the variation in deposit properties is very accurate. The horizontal measurement interval is 2.5 m, which means that after smoothing the distribution of sulphur content by using a running average, those areas with definitely increased sulphur content can be indicated with a high degree of confidence.
- (5) The estimation of porosity values based on the amplitude reflected from the top of the carbonate deposit appears to be affected by a smaller error than in the case of seismic inversion.

Author Contributions: Conceptualization, K.C. and J.D.; methodology, K.C. and J.D.; software, K.C.; validation, J.D.; formal analysis, K.C. and J.D.; investigation, K.C. and J.D.; resources, K.C. and J.D.; data curation, J.D.; writing—original draft preparation, K.C.; writing—review and editing, K.C.; visualization, J.D.; supervision, J.D.; project administration, J.D.; funding acquisition, J.D. Both authors have read and agreed to the published version of the manuscript.

Funding: The research was supported by Grupa Azoty-Siarkopol S.A., the owner of the Osiek sulphur mine, AGH University of Science and Technology in Krakow (Poland) grant number 16.16.140.315 and Initiative for Excellence - Research University at AGH UST.

Acknowledgments: We thank the Geophysical Services Company Geokar-PBG sp. z O.O. for providing all the necessary well data. Vista 2D/3D Seismic Data Processing and the Hampson-Russell Suite were provided by Schlumberger and CGG through the University Software Donation Program. We would also like to thank the four anonymous reviewers for providing valuable and insightful feedback on the manuscript.

Conflicts of Interest: The authors declare no conflict of interest.

Abbreviations

R^2	coefficient of determination
P-wave	compressional wave
S-wave	shear wave
CMP	common mid-point
NMO	normal move-out
RAP	relative amplitude preservation
V_p	P-wave velocity of rock
V_{sulph}	P-wave velocity of sulphur
V_w	P-wave velocity of water
V_m	P-wave velocity of limestone skeleton
V_{NMO}	normal move-out velocity
ϕ	porosity
φ_{sulph}	sulphur content
φ_c	clay content
ρ	bulk density
ρ_f	density of the medium saturating the pore space
ρ_m	density of the rock skeleton
ρ_w	density of the water
ρ_{sulph}	density of the sulphur
ρ_c	density of the clay
ρ_l	density of the limestone
r	reflection coefficient
$A(x_{well})$	amplitude from the deposit recorded at the position “x” of borehole
r_{well}	value of the reflection coefficient from the deposit at the position of borehole

References

1. Rogacki, H. Polish industry in the transformation period. In *Poland in the Geographical Centre of Europe*; Czerny, M., Ed.; Nova Science Publishers, Inc.: New York, NY, USA, 2006; pp. 89–114.
2. Gorylewski, E.; Bobrowska-Krajewska, K. Możliwości dalszej produkcji siarki kopalnej w Polsce na tle światowych tendencji jej pozyskiwania i zastosowania. *Przemysł Chem.* **2000**, *79*, 147–149. (In Polish)
3. Harraz, H.Z. Sulphur Ore Deposits. Prof. Dr. H.Z. Harraz Presentation. Available online: https://www.researchgate.net/publication/301860125_Sulphur_Ore_Deposits (accessed on 2 August 2021).
4. Barton, L. *Sulfate-Reducing Bacteria*; Springer: New York, NY, USA, 1995.
5. Labrado, A.L.; Brunner, B.; Bernasconi, S.M.; Peckmann, J. Formation of Large Native Sulfur Deposits Does Not Require Molecular Oxygen. *Front. Microbiol.* **2019**, *10*, 1–26. [CrossRef] [PubMed]
6. Bolewski, A. *Surowce Mineralne Świata. Siarka, Mineralogia i Petrografia*; Wyd. Geologiczne: Warszawa, Polska, 1986. (In Polish)
7. Bońda, R. Siarka. In *Bilans Zasobów złóż Kopalin w Polsce wg Stanu na 31.XII.2020r*; Szufflicki, M., Malon, A., Tymiński, M., Eds.; PIG-PIB: Warszawa, Poland, 2021; pp. 75–78. (In Polish)
8. Dec, J. Seismic monitoring of hole exploitation of sulfur deposit. *Gospod. Surowcami Miner.* **2008**, *24*, 199–213. (In Polish)

9. Dec, J. High resolution seismic investigations for the determination of water flow directions during sulphur deposits exploitation. *Acta Geophys.* **2010**, *58*, 5–14. [[CrossRef](#)]
10. Dec, J. *High-Resolution Seismic Survey for Recognition of the Osiek Sulphur Deposits and Determination of Dynamic Changes Resulting from Exploitation*; Wydawnictwa AGH: Kraków, Poland, 2012. (In Polish)
11. Dec, J.; Cichostępski, K. Evaluation of sulphur deposit properties on the basis of geomechanical parameters. *Zesz. Nauk. Inst. Gospod. Surowcami Miner. Energii PAN* **2017**, *101*, 203–216. (In Polish with English Abstract)
12. Dec, J.; Cichostępski, K. Estimation of sulphur deposit resources on the basis of seismic data. *Zesz. Nauk. Inst. Gospod. Surowcami Miner. Energii PAN* **2017**, *101*, 217–227. (In Polish with English Abstract)
13. Cichostępski, K.; Dec, J.; Kwietniak, A. Simultaneous Inversion of Shallow Seismic Data for Imaging of Sulfurized Carbonates. *Minerals* **2019**, *9*, 203. [[CrossRef](#)]
14. Brigaud, B.; Benoit, V.; Durllet, C.; Decinincq, J.; Blanc, P.; Trouiller, A. Acoustic Properties of Ancient Shallow-Marine Carbonates: Effects of Depositional Environments and Diagenetic Processes (Middle Jurassic, Paris Basin, France). *J. Sediment. Res.* **2008**, *80*, 791–807. [[CrossRef](#)]
15. Li, Y.Y.; Downton, J. Application of amplitude versus offset in carbonate reservoirs: Re-examining the potential. *SEG Tech. Program Expand. Abstr.* **2000**, 166–169. [[CrossRef](#)]
16. Dong, W.; Tura, A.; Sparkman, G. An introduction—Carbonate geophysics. *Lead. Edge* **2003**, *22*, 637–638. [[CrossRef](#)]
17. Chopra, S.; Chemingui, N.; Miller, R.D. An introduction to this special section—Carbonates. *Lead. Edge* **2005**, *24*, 488–489. [[CrossRef](#)]
18. Rafavivh, F.; Kendall, C.C.; Todd, T.P. Relation between the Acoustic Properties and the Petrographic Character of Carbonate Rocks. *Explor. Geophys.* **1984**, *49*, 1622–1636. [[CrossRef](#)]
19. Campbell, S.J.; Graval, N. The prediction of high porosity chalks in the East Hod field. *Pet. Geosci.* **1995**, *1*, 57–70. [[CrossRef](#)]
20. Cichostępski, K.; Dec, J.; Kwietniak, A. Relative amplitude preservation in high-resolution reflection seismic: A case study from Fore-Sudetic Monocline, Poland. *Acta Geophys.* **2019**, *67*, 77–94. [[CrossRef](#)]
21. Resnick, J.R. Seismic data processing for AVO and AVA analysis. In *Offset-Dependent Reflectivity—Theory and Practice of AVO Analysis*; Castagna, J.P., Backus, M.M., Eds.; SEG: Tulsa, OK, USA, 1993; pp. 175–189.
22. Chopra, S.; Castagna, J.P. *AVO*; SEG: Tulsa, OK, USA, 2014.
23. Oszczytko, N.; Krzywiec, P.; Popadyuk, I.; Peryt, T. Carpathian Foredeep Basin (Poland and Ukraine): Its Sedimentary, Structural, and Geodynamic Evolution. In *The Carpathians and Their Foreland: Geology and Hydrocarbon*; Golonka, J., Picha, F.J., Eds.; AAPG: Tulsa, OK, USA, 2006; pp. 293–350.
24. Cichostępski, K.; Kwietniak, A.; Dec, J. Verification of bright spots in the presence of thin beds by AVO and spectral analysis in Miocene sediments of Carpathian Foredeep. *Acta Geophys.* **2019**, *67*, 1731–1745. [[CrossRef](#)]
25. Marzec, P.; Sechman, H.; Kasperska, M.; Cichostępski, K.; Guzy, P.; Pietsch, K.; Porebski, S.J. Interpretation of a gas chimney in the Polish Carpathian Foredeep based on integrated seismic and geophysical data. *Basin Res.* **2018**, *30*, 210–222. [[CrossRef](#)]
26. Dziadzio, P.; Maksym, A.; Olszewska, B. Miocene deposition in the eastern part of the Carpathian Foredeep in Poland. *Przegląd Geologiczny* **2006**, *54*, 413–420.
27. Serra, O. *Fundamentals of Well-Log Interpretation—Part 1*; Elsevier: New York, NY, USA, 1984.
28. Jarzyna, J.; Bała, M. Measurements and interpretation of well logs in the Jeziórko sulphur deposit, Tarnobrzeg, Poland. *Geol. Q.* **2000**, *44*, 157–166.
29. Wyllie, M.R.J. An experimental investigation of factors affecting elastic wave velocities in porous media. *Geophysics* **1958**, *23*, 459–494. [[CrossRef](#)]
30. Gardner, G.H.F.; Gardner, L.W.; Gregory, A.R. Formation velocity and density—The diagnostic basis for stratigraphic traps. *Geophysics* **1974**, *39*, 770–780. [[CrossRef](#)]
31. Yilmaz, Ö. *Seismic Data Analysis*; Society of Exploration Geophysicists: Tulsa, OK, USA, 2001.
32. Malehmir, A.; Durrheim, R.J.; Bellefleur, G.; Urosevic, M.; Juhlin, C.; White, D.; Milkereit, B.; Campbell, G. Seismic methods in mineral exploration and mine planning, a general overview of past and present case histories and a look into the future. *Geophysics* **2012**, *77*, WC173–WC190. [[CrossRef](#)]
33. Singh, B.; Malinowski, M.; Hloušek, F.; Koivisto, E.; Heinonen, S.; Hellwig, O.; Buske, S.; Chamarczuk, M.; Juurela, S. Sparse 3D Seismic Imaging in the Kylylahti Mine Area, Eastern Finland: Comparison of Time Versus Depth Approach. *Minerals* **2019**, *9*, 305. [[CrossRef](#)]
34. Golonka, J.; Pietsch, K.; Marzec, P.; Kasperska, K.; Dec, J.; Cichostępski, K.; Lasocki, S. Deep structure of the Pieniny Klippen Belt in Poland. *Swiss J. Geosci.* **2019**, *112*, 475–506. [[CrossRef](#)]
35. Benjumea, B.; Teixido, T. Seismic reflection constraints on the glacial dynamics of Johnsons Glacier. *Antarct. J. Appl. Geophys.* **2001**, *46*, 31–44. [[CrossRef](#)]
36. Francese, R.G.; Hajnal, Z.; Schmitt, D.; Zaja, A. High resolution seismic reflection imaging of complex stratigraphic features in shallow aquifers. *Memorie Descrittive della Carta Geologica d'Italia* **2007**, *LXXVI*, 175–192.
37. Leucci, G. Geophysical investigations to study the physical–mechanical characteristics of the rock in a coastal environment: The cliff of Roca (Lecce, Italy). *J. Geophys. Eng.* **2007**, *4*, 462–475. [[CrossRef](#)]
38. Dehghannejad, M.; Malehmir, A.; Svensson, M.; Lindén, M.; Möller, H. High-resolution reflection seismic imaging for the planning of a double-track tunnel in the city of Varberg, southwest Sweden. *Near Surf. Geophys.* **2017**, *15*, 226–240. [[CrossRef](#)]
39. Singh, S. High-frequency shallow reflection mapping in tin mining. *Geophys. Prospect.* **1984**, *32*, 1033–1044. [[CrossRef](#)]

40. Palmer, D. High resolution seismic reflection surveys for coal. *Geoexploration* **1987**, *24*, 397–408. [[CrossRef](#)]
41. Tselentis, A.; Paraskevopoulos, P. Application of a high-resolution seismic investigation in a Greek coal mine. *Geophysics* **2002**, *67*, 50–59. [[CrossRef](#)]
42. Prabhakara, P.P.; Dhanam, K.; Pavan, P.K.; Mysaiah, D.; Seshunarayana, T. High resolution seismic reflection studies in Godavari coal fields: Mapping of coal seams and associated structural features. *J. Geol. Soc. India* **2015**, *86*, 317–323. [[CrossRef](#)]
43. Missiaen, T.; Murphy, S.; Loncke, L.; Henriët, J.P. Very high-resolution seismic mapping of shallow gas in the Belgian coastal zone. *Cont. Shelf Res.* **2002**, *22*, 2291–2301. [[CrossRef](#)]
44. Darling, T. *Well Logging and Formation Evaluation*; Elsevier: New York, NY, USA, 2005.
45. Asquith, G.B.; Krygowski, D. *Basic Well Log Analysis*, 2nd ed.; AAPG: Tulsa, OK, USA, 2004.
46. Aki, K.; Richards, P.G. *Quantitative Seismology*; Freeman and Co.: New York, NY, USA, 1980.
47. Shuey, R.T. A simplification of the Zoeppritz equations. *Geophysics* **1985**, *50*, 609–617. [[CrossRef](#)]
48. Zoeppritz Explorer Applet. Consortium for Research in Elastic Wave Exploration Seismology. University of Calgary. Available online: <https://www.crewes.org/ResearchLinks/ExplorerPrograms/ZE> (accessed on 2 August 2021).
49. Knapp, R.W.; Steeples, D.W. High-resolution common-depth-point seismic reflection profiling: Instrumentation. *Geophysics* **1986**, *51*, 276–282. [[CrossRef](#)]
50. Henley, D.C. Coherent noise attenuation in the radial trace domain. *Geophysics* **2003**, *68*, 1408–1416. [[CrossRef](#)]
51. Taner, M.T.; Koehler, F. Surface consistent corrections. *Geophysics* **1981**, *46*, 17–22. [[CrossRef](#)]
52. Pendrel, J. Seismic inversion—Still the best tool for reservoir characterization. *Can. Soc. Explor. Geophys. Rec.* **2001**, *26*, 5–12.
53. Cichostępski, K.; Kwietniak, A.; Dec, J.; Kasperska, M.; Pietsch, K. Integrated geophysical data for sweet spot identification in Baltic Basin, Poland. *Ann. Soc. Geol. Pol.* **2019**, *89*, 215–231. [[CrossRef](#)]
54. Veeken, P.C.H.; Da Silva, M. Seismic inversion methods and some of their constraints. *First Break* **2004**, *22*, 47–70. [[CrossRef](#)]
55. Kwietniak, A.; Cichostępski, K.; Kasperska, M. Resolution enhancement with relative amplitude preservation for unconventional targets. *Interpretation* **2018**, *6*, SH59–SH71. [[CrossRef](#)]
56. Li, Y.; Downton, J.; Goodway, W. Recent applications of AVO to carbonate reservoirs in the Western Canadian sedimentary basin. *Lead. Edge* **2003**, *22*, 670–675. [[CrossRef](#)]
57. Ishiyama, T.; Ikawa, H.; Belaid, K. AVO applications for porosity and fluid estimation of carbonate reservoirs offshore Abu Dhabi. *First Break* **2010**, *29*, 93–100. [[CrossRef](#)]
58. Hampson, D.P.; Russell, B.H.; Bankhead, B. Simultaneous inversion of pre-stack seismic data. *SEG Tech. Program Expand. Abstr.* **2005**, 1633–1637. [[CrossRef](#)]
59. Kwietniak, A.; Cichostępski, K.; Kasperska, M. Spectral Decomposition Using the CEEMD Method: A Case Study from the Carpathian Foredeep. *Acta Geophys.* **2016**, *64*, 1525–1541. [[CrossRef](#)]